Two distinct rotations of bithiazole DNA intercalation revealed by direct comparison of crystal structures of Co(III)•bleomycin A_2 and B_2 bound to duplex 5´-TAGTT sites

Kristie D. Goodwin[a], Mark A. Lewis[b], Eric C. Long[b, *], Millie M. Georgiadis[a, *]

[a]Department of Biochemistry & Molecular Biology, Indiana University School of Medicine, Indianapolis, IN, 46202, USA

[b]Department of Chemistry & Chemical Biology, Indiana University–Indianapolis (IUPUI), 402 North Blackford Street, Indianapolis, Indiana 46202, USA

*Corresponding authors.
Email addresses: mgeorgia@iu.edu (M.M. Georgiadis), eclong@iu.edu (E.C. Long)

ARTICLE INFO
Keywords: DNA binding, antitumor agent, intercalation, bleomycin

ABSTRACT

Bleomycins constitute a family of anticancer natural products that bind DNA through intercalation of a C-terminal tail/bithiazole moiety and hydrogen-bonding interactions between the remainder of the drug and the minor groove. The clinical utility of the bleomycins is believed to result from single- and double-strand DNA cleavage mediated by the HOO-Fe(III) form of the drug. The bleomycins also serve as a model system to understand the nature of complex drug-DNA interactions that may guide future DNA-targeted drug discovery. In this study, the impact of the C-terminal tail on bleomycin-DNA interactions was investigated. Toward this goal, crystal structures of HOO-Co(III)•$BLMA_2$ "green" (a stable analogue of the active HOO-Fe(III) drug) bound partially in one and fully in a second structure to duplex 5´-TAGTT sites were determined. The structures reported here were captured by soaking HOO-Co(III)•$BLMA_2$ into preformed host-guest crystals including a preferred DNA-binding site. While the overall structures of the DNA-bound metal binding domain, disaccharide, and linker peptide of $BLMA_2$ were found to be similar to those reported earlier at the same DNA site for $BLMB_2$, *the intercalated bithiazole of $BLMB_2$ is actually "flipped" 180˚ relative to DNA-bound $BLMA_2$*. This is true both in the partially and fully bound structures and highlights an until now unidentified role for the C-terminal tail in directing the intercalation of the bithiazole. In addition, these analyses identified specific bond rotations within the C-terminal domain of the drug that may be relevant for its reorganization and ability to carry out a double-strand DNA cleavage event.

1. Introduction

Bleomycins (BLMs) were first isolated over fifty years ago[1, 2] from *Streptomyces verticillus* and constitute a family of structurally related glycopeptide natural products with clinical antitumor activity[3, 4] (Fig. 1). The clinical efficacy of the BLMs is believed to derive from the ability of these agents to induce oxidative DNA strand scission[5] leading to single- *and* double-strand[6] DNA cleavage events. Of these DNA lesions, the latter are considered to be the primary cause of BLM cytotoxicity and a likely basis for their antitumor activity. In addition to their clinical relevance, from a fundamental scientific perspective, investigation of the BLMs[7-11] has provided an essential paradigm towards the design of DNA-interactive entities.[12] Despite years of effort, however, our knowledge of several basic aspects of the BLM-DNA interaction remains incomplete.[10, 13] For example, while models[14, 15] to explain the DNA cleavage activities of this drug have been influenced by evidence suggesting alternative drug-DNA binding modes[16, 17] details of these binding modes and possible accompanying structural reorganizations[14] remain to be verified experimentally.

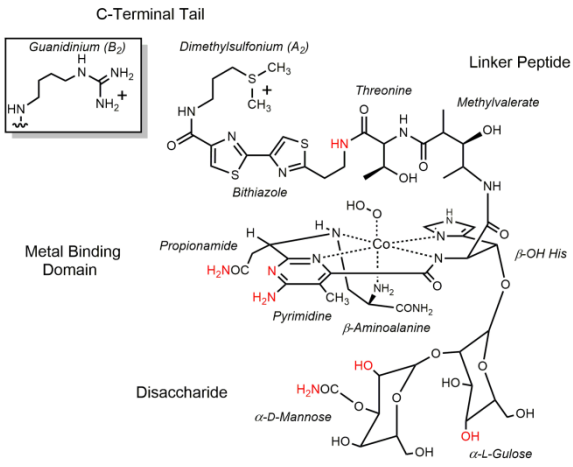

Fig. 1 Schematic of Co•$BLMA_2$. The structure of $BLMA_2$ includes a disaccharide, metal-binding domain, linker peptide, bithiazole, and C-terminal dimethylsulfonium moiety that differs among drug congeners; the B_2 congener (see inset) displays a C-terminal guanidinium moiety. Atoms depicted in red mediate intermolecular H-bonding between Co•$BLMA_2$ and DNA.

This is the author's manuscript of the article published in final edited form as:

Goodwin, K. D., Lewis, M. A., Long, E. C., & Georgiadis, M. M. (2023). Two distinct rotations of bithiazole DNA intercalation revealed by direct comparison of crystal structures of Co(III)•bleomycin A2 and B2 bound to duplex 5'-TAGTT sites. Bioorganic & Medicinal Chemistry, 77, 117113. https://doi.org/10.1016/j.bmc.2022.117113

Towards our understanding of bleomycin, we reported the first crystal structures of Co(III)•$BLMB_2$ bound to a DNA oligonucleotide.[18] These structures revealed several features which differed from previous investigations[19, 20] including: (1) the intermolecular interactions observed to form at a preferred 5′-GT leading to bithiazole-DNA intercalation; (2) a detailed description of the impact of drug binding on the structure of the DNA substrate; and (3) a determination that drug binding occurs over a five base-pair DNA "footprint". In this current study, the structural characterization of $BLMA_2$ and a comparative analysis with $BLMB_2$ structures has revealed rotation of the intercalated bithiazole/C-terminal moiety relative to the rest of the drug, which promotes stable drug-DNA binding in each of the two congeners with DNA.

2. Materials and Methods

2.1. Crystallization

DNA oligonucleotides were purchased from IDT and used without further purification. The N-terminal fragment (residues 24-278) of Moloney murine leukemia virus reverse transcriptase (referred to here as RT) was purified, and RT-DNA crystals were grown as previously described.[19-21] BLM A_2 was fractionated[22] from commercially-available blenoxane, metallated as described previously,[23, 24] purified by HPLC, and verified by LC-MS.

Crystals were obtained with two different self-complementary oligonucleotides d(ATTA**GT**TATAACTAAT)$_2$ **(1)** or d(CTTA**GT**TATAACTAAG)$_2$ (**1C**). The structure of RT:**1** denoting RT complexed with oligonucleotide **1** has been previously reported (2R2R). The structure of RT:**1C** is reported here for comparison with the RT:**1C**-BLM complex. To obtain complexes with BLM, crystals were soaked in solutions containing 9% PEG 4000, 5 mM magnesium acetate, 100 mM HEPES pH 8.0, and 0.1 mM BLM followed by stabilization in a cryosolvent including 20% ethylene glycol and 0.25 mM BLM. Sets of crystals were soaked in BLM for intervals of 1 hour and tested by diffraction for unit cell changes. Data were collected when changes in either one or all three cell parameters were apparent upon initial indexing of the crystals in HKL2000.[25]

2.2. Data Collection and Refinement

Data were collected at the SBC beamline 19-ID of the Advanced Photon Source (Argonne, IL), integrated and processed with the HKL2000 package.[25] Crystal structures were determined by molecular replacement with PHASER[26] using the refined model of the N-terminal fragment of MMLV RT as the search model (1ZTW) to obtain unbiased electron density of the DNA and drug. Coordinates for the B-form model of the desired DNA sequence were generated using Nucleic Acid Builder.[27] Following addition of well-ordered water molecules, the first three base pairs that contact RT directly were adjusted manually in COOT[28] to fit the electron density, followed by cycles of refinement and then addition of the next two base pairs and finally the remainder of the DNA along with BLM.

For the fully bound structure RT:**1C** (**Fig. 2**), the initial F_o-F_c map displayed density for the intercalated bithiazole domain, the methylvalerate portion of the linker, and the metal-binding domain and disaccharide (SI Fig. S1). Co•BLM A_2 was modeled by starting with the bleomycin A_2 coordinates from the NMR model of the drug bound to DNA (1MXK). Significant adjustments to this model were made to fit the difference electron density maps.

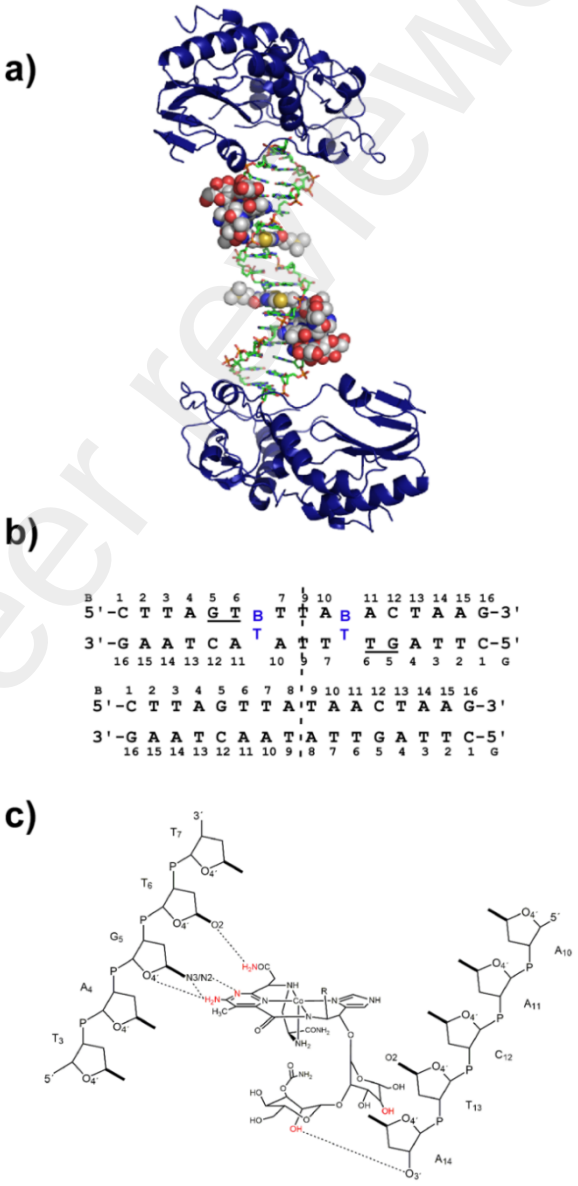

Fig. 2 Host-guest complex of $BLMA_2$ bound to DNA. (a) The host-guest complex contains the N-terminal fragment of Moloney murine leukemia virus reverse transcriptase (blue cartoon rendering), a 16 bp self-complementary oligonucleotide including a preferred 5′-GTT bleomycin binding site (green stick model), and Co(III)•$BLMA_2$ (van der Waals spheres: C, gray, O, red, N, blue, S, yellow). (b) The 16 bp oligonucleotide used for crystallization shown in the absence (bottom) and presence of $BLMA_2$ (top, BT indicates bithiazole). Two 5′-GTT sites are present in this symmetrical DNA oligonucleotide. (c) Schematic illustrating the inter-molecular H-bonding interactions observed between fully bound $BLMA_2$ and DNA (red). Dashed lines indicate interactions with nucleobase or sugar atoms. Interactions with phosphate

oxygens are not shown. Linker peptide and C-terminal tail domains not shown for clarity. See narrative for a list of detailed interactions involving these domains.

The planar bithiazole (with correct bond distances for C-S bonds) from our bleomycin B_2 structure and the C-terminal tail from 1MXK were joined to the remainder of the drug model; the hydroperoxide ligand to Co^{3+} was not observed. For refinement in PHENIX,[29] restraints files were generated for this starting BLM model with H atoms in the program PHENIX elbow and for Co(III)-ligand bond distances. Idealized bond distances, angles, and stereochemistry were corrected in the CIF file generated by the elbow program and used for refinement in PHENIX. We note that the color of the crystals did not change during the course of the X-ray experiment; we therefore conclude that exposure to X-rays has not resulted in conversion of the "green" HOO-Co(III)•BLM A_2 to the "brown" HO-Co(III)•BLM A_2 during the course of the experiment.

The initial F_o-F_c map for the intermediate structure RT:**1** displayed well-ordered density for the bithiazole with some density for the C-terminal tail. There was also a small peak of density in the minor groove, corresponding to the position of the Co^{3+} atom within the metal binding domain of the drug. No attempt was made to model additional drug moieties within the minor groove given the lack of density. Alternate cycles of model building using COOT[28] and refinement calculations in PHENIX[29] were completed until no large peaks remained in the F_o-F_c electron density maps. We refined both RT:1 and RT:**1C** structures using restrained least squares refinement with individual isotropic temperature factors. A summary of the refinement statistics is shown in Table 1. DNA structural parameters were analyzed using 3DNA.[30] Figures were generated using PYMOL.

Coordinates have been deposited with RCSB with PDB accession numbers (8DWM) for the fully bound Co•BLM A_2-DNA-RT structure, (8DW8) intermediate structure of Co•BLM A_2 bound to DNA-RT, and (8DW1) d(CTTAGTTATAACTAAG)-RT complex, sequence used to obtain the fully bound complex.

3. Results and Discussion

3.1. Crystallizations

To obtain DNA-bound $BLMA_2$ (as HOO-Co(III)•$BLMA_2$, *i.e.*, Co•$BLMA_2$ "green", **Fig. 1**), drug was soaked into host-guest crystals,[18, 31, 32] with the "host" being the N-terminal fragment of Moloney murine leukemia virus reverse transcriptase (RT) and the "guest" a self-complementary 16 base pair duplex oligonucleotide containing two drug-preferred 5′-GT sites (**Fig. 2**). It was necessary to use Co•$BLMA_2$ "green", a stable analogue[18, 33, 34] of what is considered to be the "activated" form of the drug, HOO-Fe(III)•$BLMA_2$,[35] to prevent cleavage of DNA during the crystallographic experiments.

Two oligonucleotides were examined: d(ATTA**GT**TATAACTAAT)$_2$ **(1)** and d(CTTA**GT**TATAACTAAG)$_2$ **(1C)**. A time course of soaking-in Co•$BLMA_2$ was performed, and intermediate or complete binding of Co•$BLMA_2$ was

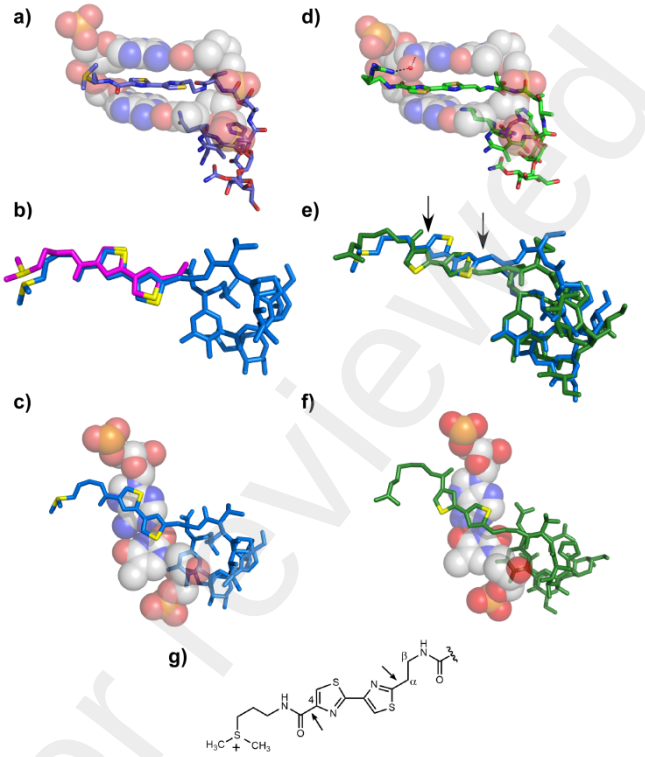

Fig. 3 The bithiazole of $BLMA_2$ intercalates in a mode flipped 180° relative to $BLMB_2$. The base pairs (van der Waal spheres) immediately above and below the site of bithiazole intercalation are shown for $BLMA_2$ (a) and $BLMB_2$ (d). BLM is shown as a stick model (C: light blue for A2, and green for B2; N: blue; O: red; S: yellow). (b) The partially bound bithiazole (magenta) is shown superimposed on the fully bound bithiazole (blue) for $BLMA_2$. $BLMA_2$ (c) and $BLMB_2$ (f) are shown as stick models (A2: blue, B2: green; S, yellow; o, red) including only the bottom nucleobase pair (van der Waals spheres) from views (a) or (d), above, rotated approximately 90°. (e) $BLMA_2$ (blue) and $BLMB_2$ (green) bound DNA modes are shown superimposed as stick models (S, yellow). Arrows indicate differences in positions of atoms in linker and C-terminal tail. (g) Schematic identifying the bonds rotated in the $BLMA_2$ structure relative to $BLMB_2$.

detected by changes in unit cell parameters (Table 1). For the fully bound (Co•$BLMA_2$:RT:**1C**) structure, all three cell parameters changed in magnitude by comparison with the unbound RT:**1C** DNA structure (a = 52.79 *vs.* 55.13 Å, b = 144.36 *vs.* 145.70 Å, and c = 49.87 *vs.* 46.87 Å for bound *vs.* unbound, respectively), while for the intermediate, partially bound structure (Co•$BLMA_2$:RT:**1**), a single cell parameter changed (b = 145.85 *vs.* 144.5 Å, bound *vs.* unbound). We report here three crystal structures: the host-guest complex RT:**1C**; an intermediate structure, Co•$BLMA_2$:RT:**1**; and a fully bound structure, Co•$BLMA_2$:RT:**1C** at 1.85, 2.6, and 3.0 Å, respectively (Table 1). RT:**1** was previously reported (PDB ID 2R2R). The structures presented here potentially represent "snapshots" in the progression of BLM binding to DNA.

In both partially and fully bound $BLMA_2$ structures, the bithiazole is intercalated in the expected site between base

pairs T_6•A_{11} and T_7•A_{10}, 3′ to the 5′-G_5T_6 site as evident in F_o-F_c difference density maps calculated prior to the inclusion of any part of Co•$BLMA_2$ in the refinement (SI, Figs. S1 and S2). Intercalation in the fully bound structure results in an increase in the rise of the base pairs at this site compared to DNA alone (drug bound DNA: T_6•A_{11}/T_7•A_{10} rise = 6.4 Å, DNA alone: T_6•A_{11} rise = 3.2 Å). In the partially bound structure, the helical rise value at the site of intercalation is similar to that in the fully bound structure (bound DNA: T_6•A_{11}/T_7•A_{10} rise = 6.7 Å, DNA alone: T_6•A_{11}/T_7•A_{10} rise = 3.2 Å).

In comparison to the structure of the DNA alone, the bithiazole is stacked between base pairs and is equivalent to one base pair step with the C-terminal tail of the drug extended into the major groove (**Figs. 2, 3a**). The asymmetric unit of RT-DNA crystals contains one RT molecule and 8 base pairs of DNA while that of the Co•$BLMA_2$ complexes includes one RT molecule, 7.5 base pairs of DNA, and one intercalated BLM. The DNA in these structures is B-form, with the exception of the sites of intercalation in the partially and fully bound bleomycin structures.

Following intercalation of the bithiazole, adenines from the A-T base pairs at the dyad extrude resulting in a T-T base pair as reported previously for the Co•$BLMB_2$-DNA structures.[18] To accommodate the bithiazole, the DNA in the fully bound structure is overwound for dinucleotide step G_5•C_{12}/T_6•A_{11} by 4.9° and underwound by 10.1° at the site of intercalation T_6•A_{11}/T_7•A_{10}. For the partially bound structure, the helical twist is underwound by 6.5° for dinucleotide step A_4•T_{13}/G_5•C_{12}, overwound for dinucleotide step G_5•C_{12}/T_6•A_{11} by 4.8° and underwound by 5.7° at the site of intercalation T_6•A_{11}/T_7•A_{10}. The average helical twist in the fully and partially bound structures are similar, 34° and 32°, respectively. These differences in helical twist between the two structures may reflect real changes in the structure of the DNA that are required to fully accommodate binding of Co•$BLMA_2$. In addition, the DNA minor groove width is also affected by interactions with Co•$BLMA_2$: the minor grooves in both the fully bound and partially bound structures are widened by approximately 2 Å as compared to the same DNA oligonucleotide in the absence of bound drug. This finding suggests that although not fully ordered in the partially bound structure, the metal-binding domain and disaccharide interact with the minor groove.

The overall structure of the fully bound Co•$BLMA_2$-RT:**1C** DNA complex is similar to that of the previously reported Co•$BLMB_2$-DNA complex[18] with metal coordinating ligands forming a distorted square pyramidal structure as shown in Fig. 1. Electron density was apparent for all drug moieties excluding the propionamide and the hydroperoxide ligand (SI Fig. S1); the propionamide and the hydroperoxide were modelled based on coordinates in the NMR structure (1MXK). In our model, the distal oxygen of the hydroperoxide is 2.4 Å from the C4′-H, the target of drug-DNA oxidation,[7-11] and is thus appropriately poised for H abstraction (SI Fig. S3). The metal-binding domain and disaccharide bind in the minor groove. A total of 10 possible hydrogen-bonding interactions with the DNA involve the metal-binding domain, linker, and disaccharide of Co•$BLMA_2$ (Table 2). There are three nucleobase-specific minor groove interactions, one involving the NH_2 (NF) group of the metal-binding domain pyrimidine to N3 of G_5, a second potential interaction involving NH_2 (N2) of G_5 with NE of the pyrimidine, and a third interaction between the propionamide NH_2 with O2 of T_6 (Fig. 2c, Table 2). Other non-nucleobase specific hydrogen bonds occur between the drug and the sugar-phosphate backbone. These include the pyrimidine C4-NH_2 to O4′ of G_5, the β-aminoalanine NH_2 to O3′ of T_{13} and O4′ of A_{14}, the amide NH linking threonine to the bithiazole to the O4′ of T_7, the α-D-mannose C2-OH to OP1 of A_{15} and O3′ of A_{14}, and the α-L-gulose CH_2-OH to OP1 of A_{14}. Many of the hydrogen-bonding interactions between $BLMA_2$ and the DNA observed here were also observed in the $BLMB_2$-DNA complex, a significant exception being differences involving the C-terminal tail.

Upon DNA binding, each new $BLMA_2$ structure was observed to orient its intercalated bithiazole into the DNA helical stack, albeit with slight differences (Fig. 3a-c). Relative to the positioning of the bithiazole ring observed in the *fully* bound $BLMA_2$ structure, in the *partially* bound structure of $BLMA_2$ to **1**, this bithiazole is oriented similarly but is shifted approximately 0.5 Å toward the minor groove face (Fig. 3b). This shift from the partially bound to the fully bound structure effectively brings the metal-binding domain of the fully bound structure closer to its target sequence and appears to "complete" the binding process. Thus, overall, the orientations of the DNA bound bithiazoles observed in both new Co•$BLMA_2$ structures are similar to the orientations observed in NMR structures[33, 34] of Co•$BLMA_2$ bound to DNA sites different from the 5′-GTT site examined here.

Of further mechanistic significance concerning the bithiazole, a full comparison of the $BLMA_2$ and $BLMB_2$ structures now in hand (Fig. 3) revealed two significant differences. The bithiazoles in these new Co•$BLMA_2$ crystal structures (and all other reported $BLMA_2$ structures) are rotated relative to their counterparts observed in our Co•$BLMB_2$ crystal structures; the bithiazole insertion observed in $BLMB_2$ is "flipped" 180° in comparison to our $BLMA_2$ structures at the same DNA site. In addition, the C-terminal thiazole ring of $BLMB_2$ is shifted towards the major groove by approximately 2.5 Å while the N-terminal thiazole rings in each structure superimpose well (albeit, flipped) in the two different DNA-bound congeners (**Fig. 3e**).

The "flipped" bithiazole insertion revealed for $BLMB_2$ relative to $BLMA_2$ occurs through rotation of the bond connecting the C-α methylene linker of the Thr residue to the C2′-position of the amino terminal thiazole ring relative to its position in the A_2 congener crystal structures (**Fig. 3e, g**). Rotation at this drug position located in the DNA minor groove is accompanied by an additional rotation of the bond connecting the C-terminal thiazole ring C4 to the carbonyl carbon of its peptide link to the C-terminal moiety located in the major groove. In the case of $BLMA_2$, rotation of the intercalated bithiazole appears to allow the bithiazole to stack more optimally between A_{11} and A_{10} on the strand complementary to the 5′-GTpT recognition site relative to the stacking observed with the B_2 bithiazole at this same site (Fig. 3c, f).

Along with the differences described above for the bithiazole, the C-terminal dimethylsulfonium tail of $BLMA_2$ lacks hydrogen-bonding interactions with the DNA (Fig. 3a, d). In contrast, the C-terminal guanidinium of Co•$BLMB_2$ was observed[18] to form a water-mediated interaction with the N7 atom of A_{10} in the DNA major groove. Lacking the C-terminal tail anchoring point observed in our analysis of $BLMB_2$ (that served to maintain a deep insertion of the $BLMB_2$ bithiazole resulting in the 2.5 Å shift towards the major groove noted earlier), the less deeply inserted bithiazole of $BLMA_2$ appears in comparison to be able to achieve greater stacking with the complementary strand ApA purines of the 5′-GTT target site. Thus, it appears that the chemical nature of the C-terminal tail, *i.e.*, guanidinium *vs*. dimethylsulfonium, influences the behavior and positioning of the bithiazole to an extent greater than traditionally viewed.

4. Conclusions

This second structural analysis of a BLM congener (Co•$BLMA_2$) in partially and fully DNA-bound states reinforces a model in which full intercalation of the bithiazole mediates engagement of the metal-binding domain with the minor groove. In partially bound structures, the metal binding domain is disordered, presumably because it does not yet form specific interactions with the DNA. Also, as reported for the Co•$BLMB_2$ congener, intercalation of the bithiazole moiety appears to be the preferred binding mode for Co•$BLMA_2$, and our host guest system allows each congener to adopt its preferred orientation for the bithiazole moiety. No doubt DNA sites containing different sequences will lead to alternative interactions suggesting that a family of versatile bithiazole/C-terminal domains has evolved to accommodate and support a multitude of drug-DNA binding scenarios.

As a final note, we suggest that the ability to "flip" the bithiazole/C-terminus of BLM by 180˚ (via the bonds noted earlier) and to bind DNA in either bithiazole orientation bears a striking relevance to one of several models developed to explain the double-strand DNA cleavage activity of the bleomycins. However, while the "reorganization model"[10, 14, 15, 36] predicted 180˚ rotation about the thiazole-thiazole connecting bond as a means to access two DNA cleavage sites adjacent to a single location of BT intercalation, our crystallization studies have clearly identified a different drug location where rotation actually occurs. Of additional relevance to double-strand DNA cleavage, in our intermediate structure with a partially intercalated BT, the metal binding domain is disordered and lacks a fully stable association with the DNA minor groove. While only conjecture, this partially intercalated state may lead to increased solvent accessibility of the metal binding domain. This latter observation supports a possible pathway that permits DNA-bound drug activation, or the drug "reactivation" required to induce a double-strand cleavage lesion. Finally, now having examined two distinctly different BLM congeners, it appears likely that the nature of the C-terminal tail of bleomycin and its mode of DNA anchoring may exert profound influence over this process. There is, however, little doubt that different target DNA sequences beyond those studied to date will influence the choice of binding modes available to BLM and that wholly alternative binding modes may exist and await verification.

Declaration of Competing Interest

The authors declare that they have no known competing financial interests or personal relationships that could have appeared to influence the work reported in this paper.

Acknowledgement

We thank Marianne Cuff, Steve Ginell, and Andrzej Joachimiak from the Structural Biology Center Collaborative Access Team at the Advanced Photon Source. Results shown in this report are derived from work performed at Argonne National Laboratory, Structural Biology Center at the Advanced Photon Source. Argonne is operated by UChicago Argonne, LLC, for the U.S. Department of Energy, Office of Biological and Environmental Research under Contract DE-AC02-06CH11357. This work was supported by a fellowship from the American Cancer Society (to K.D.G.).

Appendix A. Supplementary material

Supplementary data to this article can be found online at https://doi. org/

References

1. H. Umezawa, Bleomycin and other antitumor antibiotics of high molecular weight, *Antimicrob Agents Chemother (Bethesda)*, 1965; 5, 1079-1085. https://www.ncbi.nlm.nih.gov/pubmed/5883403.
2. H. Umezawa, K. Maeda, T. Takeuchi, Y. Okami, New antibiotics, bleomycin A and B, *J Antibiot (Tokyo)*, 1966; 19, (5) 200-209. https://www.ncbi.nlm.nih.gov/pubmed/5953301.
3. L.H. Einhorn, Curing metastatic testicular cancer, *Proc Natl Acad Sci U S A*, 2002; 99, (7) 4592-4595. https://www.ncbi.nlm.nih.gov/pubmed/11904381.
4. J.M. Connors, State-of-the-art therapeutics: Hodgkin's lymphoma, *J Clin Oncol*, 2005; 23, (26) 6400-6408. https://www.ncbi.nlm.nih.gov/pubmed/16155026.
5. K. Nagai, H. Yamaki, H. Suzuki, N. Tanaka, H. Umezawa, The combined effects of bleomycin and sulfhydryl compounds on the thermal denaturation of DNA, *Biochim Biophys Acta*, 1969; 179, (1) 165-171. https://www.ncbi.nlm.nih.gov/pubmed/4892115.
6. L.F. Povirk, W. Wubter, W. Kohnlein, F. Hutchinson, DNA double-strand breaks and alkali-labile bonds produced by bleomycin, *Nucleic Acids Res*, 1977; 4, (10) 3573-3580. https://www.ncbi.nlm.nih.gov/pubmed/73164.
7. D.L. Boger, H. Cai, Bleomycin: Synthetic and Mechanistic Studies, *Angew Chem Int Ed Engl*, 1999; 38, (4) 448-476. https://www.ncbi.nlm.nih.gov/pubmed/29711767.

8. C.A. Claussen, E.C. Long, Nucleic Acid recognition by metal complexes of bleomycin, *Chem Rev*, 1999; 99, (9) 2797-2816. https://www.ncbi.nlm.nih.gov/pubmed/11749501.
9. S.M. Hecht, Bleomycin: new perspectives on the mechanism of action, *J Nat Prod*, 2000; 63, (1) 158-168. https://www.ncbi.nlm.nih.gov/pubmed/10650103.
10. J. Chen, J. Stubbe, Bleomycins: towards better therapeutics, *Nat Rev Cancer*, 2005; 5, (2) 102-112. https://www.ncbi.nlm.nih.gov/pubmed/15685195.
11. S.M. Hecht, Bleomycin Group Antitumor Agents, in: G.M. Cragg, D.G.I. Kingston, D.J. Newman (Eds.) Anticancer Agents from Natural Products, CRC Press, LLC, Boca Raton, 2005, pp. 357-381.
12. B.M. Zeglis, V.C. Pierre, J.K. Barton, Metallo-intercalators and metallo-insertors, *Chem Commun (Camb)*, 2007; (44) 4565-4579. https://www.ncbi.nlm.nih.gov/pubmed/17989802.
13. M.S. Chow, L.V. Liu, E.I. Solomon, Further insights into the mechanism of the reaction of activated bleomycin with DNA, *Proc Natl Acad Sci U S A*, 2008; 105, (36) 13241-13245. https://www.ncbi.nlm.nih.gov/pubmed/18757754.
14. J. Stubbe, J.W. Kozarich, W. Wu, D.E. Vanderwall, Bleomycins: A Structural Model for Specificity, Binding, and Double Strand Cleavage, *Accounts of chemical research*, 1996; 29, (7) 322-330. https://doi.org/10.1021/ar9501333.
15. J. Chen, J. Stubbe, Bleomycins: new methods will allow reinvestigation of old issues, *Curr Opin Chem Biol*, 2004; 8, (2) 175-181. https://www.ncbi.nlm.nih.gov/pubmed/15062779.
16. J. Chen, M.K. Ghorai, G. Kenney, J. Stubbe, Mechanistic studies on bleomycin-mediated DNA damage: multiple binding modes can result in double-stranded DNA cleavage, *Nucleic Acids Res*, 2008; 36, (11) 3781-3790. https://www.ncbi.nlm.nih.gov/pubmed/18492718.
17. A.T. Abraham, X. Zhou, S.M. Hecht, Metallobleomycin-Mediated Cleavage of DNA Not Involving a Threading-Intercalation Mechanism, *Journal of the American Chemical Society*, 2001; 123, (22) 5167-5175. https://doi.org/10.1021/ja002460y.
18. K.D. Goodwin, M.A. Lewis, E.C. Long, M.M. Georgiadis, Crystal structure of DNA-bound Co(III) bleomycin B2: Insights on intercalation and minor groove binding, *Proc Natl Acad Sci U S A*, 2008; 105, (13) 5052-5056. https://www.ncbi.nlm.nih.gov/pubmed/18362349.
19. D. Sun, S. Jessen, C. Liu, X. Liu, S. Najmudin, M.M. Georgiadis, Cloning, expression, and purification of a catalytic fragment of Moloney murine leukemia virus reverse transcriptase: crystallization of nucleic acid complexes, *Protein Sci*, 1998; 7, (7) 1575-1582. http://www.ncbi.nlm.nih.gov/entrez/query.fcgi?cmd=Retrieve&db=PubMed&dopt=Citation&list_uids=9684890.
20. S. Najmudin, M.L. Cote, D. Sun, S. Yohannan, S.P. Montano, J. Gu, M.M. Georgiadis, Crystal structures of an N-terminal fragment from Moloney murine leukemia virus reverse transcriptase complexed with nucleic acid: functional implications for template-primer binding to the fingers domain, *J Mol Biol*, 2000; 296, (2) 613-632. https://www.ncbi.nlm.nih.gov/pubmed/10669612.
21. K.D. Goodwin, M.A. Lewis, F.A. Tanious, R.R. Tidwell, W.D. Wilson, M.M. Georgiadis, E.C. Long, A high-throughput, high-resolution strategy for the study of site-selective DNA binding agents: analysis of a "highly twisted" benzimidazole-diamidine, *J Am Chem Soc*, 2006; 128, (24) 7846-7854. https://www.ncbi.nlm.nih.gov/pubmed/16771498.
22. C.P. Freyder, W. Zhou, P.W. Doetsch, L.G. Marzilli, Bleomycin A2 and B2 purification by flash chromatography for chemical and biochemical studies, *Prep Biochem*, 1991; 21, (4) 257-268. http://www.ncbi.nlm.nih.gov/entrez/query.fcgi?cmd=Retrieve&db=PubMed&dopt=Citation&list_uids=1723522.
23. W. Wu, D.E. Vanderwall, C.J. Turner, J.W. Kozarich, J. Stubbe, Solution structure of Co.bleomycin A2 green complexed with d(CCAGGCCTGG), *J Am Chem Soc*, 1996; 118, 1281-1294.
24. C. Rajani, J.R. Kincaid, D.H. Petering, Resonance Raman studies of HOO-Co(III)bleomycin and Co(III)bleomycin: identification of two important vibrational modes, nu(Co-OOH) and nu(O-OH), *J Am Chem Soc*, 2004; 126, (12) 3829-3836. http://www.ncbi.nlm.nih.gov/entrez/query.fcgi?cmd=Retrieve&db=PubMed&dopt=Citation&list_uids=15038737.
25. Z. Otwinowski, W. Minor, Processing of X-ray diffraction data collected in oscillation mode, *Methods Enzymol.*, 1997; 276, 307-326.
26. A.J. McCoy, R.W. Grosse-Kunstleve, P.D. Adams, M.D. Winn, L.C. Storoni, R.J. Read, Phaser crystallographic software, *J Appl Crystallogr*, 2007; 40, (Pt 4) 658-674. https://www.ncbi.nlm.nih.gov/pubmed/19461840.
27. T. Macke, D.A. Case, Modeling unusual nucleic acid structures, in: N.B. Leontes, J. SantaLucia, J. (Eds.) Molecular Modeling of Nucleic Acids, American Chemical Society, Washington, D.C., 1998, pp. 379-393.
28. P. Emsley, K. Cowtan, Coot: model-building tools for molecular graphics, *Acta crystallographica. Section D, Biological crystallography*, 2004; 60, (Pt 12 Pt 1) 2126-2132. https://www.ncbi.nlm.nih.gov/pubmed/15572765.
29. P.D. Adams, P.V. Afonine, G. Bunkoczi, V.B. Chen, I.W. Davis, N. Echols, J.J. Headd, L.W. Hung, G.J. Kapral, R.W. Grosse-Kunstleve, A.J. McCoy, N.W. Moriarty, R. Oeffner, R.J. Read, D.C. Richardson, J.S. Richardson, T.C. Terwilliger, P.H. Zwart, PHENIX: a comprehensive Python-based system for macromolecular structure solution, *Acta crystallographica. Section D, Biological crystallography*, 2010; 66, (Pt 2) 213-221. http://www.ncbi.nlm.nih.gov/pubmed/20124702.
30. X.J. Lu, W.K. Olson, 3DNA: a software package for the analysis, rebuilding and visualization of three-dimensional nucleic acid structures, *Nucleic Acids Res*, 2003; 31, (17) 5108-5121. https://www.ncbi.nlm.nih.gov/pubmed/12930962.
31. M.L. Cote, S.J. Yohannan, M.M. Georgiadis, Use of an N-terminal fragment from moloney murine leukemia virus reverse transcriptase to facilitate crystallization and analysis of a pseudo-16-mer DNA molecule containing G-A mispairs, *Acta crystallographica. Section D, Biological crystallography*, 2000; 56, (Pt 9) 1120-1131. https://www.ncbi.nlm.nih.gov/pubmed/10957631.
32. K.D. Goodwin, E.C. Long, M.M. Georgiadis, A host-guest approach for determining drug-DNA interactions: an example using netropsin, *Nucleic Acids Res*, 2005; 33, (13) 4106-4116. https://www.ncbi.nlm.nih.gov/pubmed/16049022.
33. W. Wu, D.E. Vanderwall, C.J. Turner, J.W. Kozarich, J. Stubbe, Solution Structure of Co·Bleomycin A2 Green Complexed with d(CCAGGCCTGG), *Journal of the American Chemical Society*, 1996; 118, (6) 1281-1294. https://doi.org/10.1021/ja952497w.
34. C. Zhao, C. Xia, Q. Mao, H. Försterling, E. DeRose, W.E. Antholine, W.K. Subczynski, D.H. Petering, Structures of HO2-Co(III)bleomycin A2 bound to d(GAGCTC)2 and d(GGAAGCTTCC)2: structure–reactivity relationships of Co and Fe bleomycins, *Journal of Inorganic Biochemistry*, 2002; 91, (1) 259-268.

https://www.sciencedirect.com/science/article/pii/S0162013402004208.
35. J.W. Sam, X.-J. Tang, J. Peisach, Electrospray Mass Spectrometry of Iron Bleomycin: Demonstration That Activated Bleomycin Is a Ferric Peroxide Complex, *Journal of the American Chemical Society*, 1994; 116, (12) 5250-5256. https://doi.org/10.1021/ja00091a032.
36. D.E. Vanderwall, S.M. Lui, W. Wu, C.J. Turner, J.W. Kozarich, J. Stubbe, A model of the structure of HOO-Co·bleomycin bound to d(CCAGTACTGG): recognition at the d(GpT) site and implications for double-stranded DNA cleavage, *Chemistry & Biology*, 1997; 4, (5) 373-387. https://www.sciencedirect.com/science/article/pii/S1074552197901289.

Table 1. Summary of Crystallographic and Refinement Data

Cell Parameters	**RT:1C**	**RT:1C:A2f**	**RT:1[e]**	**RT:1:A2p**
Cell constants (Å)	*a* = 55.13	*a* = **52.79**	*a* = 55.66	*a* = 55.68
	b = 145.79	*b* = **144.36**	*b* = 144.48	*b* = **145.85**
	c = 46.87	*c* = **49.87**	*c* = 46.85	*c* = 46.82
Space Group	$P2_12_12$	$P2_12_12$	$P2_12_12$	$P2_12_12$
Statistics[a]				
Max Resolution (Å)	1.85	3.0	2.1	2.6
Reflections (unique)	33,241	8,206	22,869	12,232
(total)	165,317	31,580	82,307	50,788
Completeness (%)	98.7 (90.5)	93.8 (63.8)	95.7 (76.4)	95.2 (97.3)
R*sym* (%) [b]	5.3 (47.2)	8.6 (28.9)	7.0 (44.4)	10.1 (62.7)
I/σI	27.1 (2.1)	14.2 (2.9)	14.3 (1.7)	13.2 (2.1)
Refinement				
Resolution range (Å)	50-1.85	50-3.0	50–2.1	50–2.6
R*value* (%)[d]	20.0	22.5	23.8	22.1
R*free* (%)	23.9	29.7	26.9	27.6
RMSD				
Bond (Å)	0.006	0.004	0.006	0.004
Angle (°)	1.10	0.92	1.29	0.71
Average B-factor (Å²)[c]				
Protein	31.1	42.6	41.7	54.1
DNA	50.5 (325)	81.39 (304)	52.8 (325)	80.5 (304)
Water	37.3 (309)		37.6 (168)	38.6 (21)
BLM	N/A	83.7 (99)	N/A	99.0 (21)

[a]Data in ( ) are for highest resolution shell.
[b] $R_{sym} = \Sigma\Sigma_i|I_i - \langle I \rangle| / \Sigma\langle I \rangle$ where I is the integrated intensity of a reflection.
[c]Data in ( ) is the number of atoms.
[d] $R_{value} = \Sigma_{hkl}||F_{obs} - kF_{calc}|/\Sigma_{hkl}|F_{obs}|$. 5% of all reflections were omitted from refinement; R_{free} is the same statistic calculated for these reflections.
[e]Previously reported structure and data.[18]
Abbreviations: btd, bithiazole domain; mbd, metal-binding domain; dsd, disaccharide domain; A2f, A2 fully bound drug; A2p, A2 partially bound drug.

Table 2. Hydrogen bonds between Co•BLM A_2 and DNA			
BLM atom	**DNA atom**	**Chain**	**Distance (Å)**
Metal binding domain			
Pyrimidinyl propionamide			
pyrimidine N3 (NE)	**N2 of G5**	B	3.5*
pyrimidine C4-NH_2 (NF)	O4' of G5	B	3.1
	N3 of G5	B	2.8
propionamide NH_2 (ND)	O2 of T6	B	3.2*
β-aminoalanine NH_2 (NA)	O3' of T13	G	2.1**
	O4' of A15	G	3.0
Linker			
Threonine			
(amide link to bithiazole, NM)	O4' of T7	B	3.2
Disaccharide			
Gulose			
C2-OH (O59)	OP1 of A14	G	2.9
Mannose			
C2-OH (O69)	OP1 of A15	G	2.8
C2-OH (O69)	O3' of A14	G	2.8

Atom names given are those found in the coordinate file. Base specific interactions with DNA are denoted in bold in the DNA atom column. * Possible h-bonding interaction; ** close contact in current model, possible h-bonding interaction.